

Repositioning Therapeutics for COVID-19: Virtual Screening of the Potent Synthetic and Natural Compounds as SARS-CoV-2 3CLpro Inhibitors

Ahmad Sattari

University of Zanjan

Ali Ramazani (✉ aliramazani@gmail.com)

University of Zanjan

Hamideh Aghahosseini

University of Zanjan

Research Article

Keywords: COVID-19, Drug discovery, Medicinal chemistry, Molecular docking, Synthetic and natural ligands

Posted Date: June 30th, 2020

DOI: <https://doi.org/10.21203/rs.3.rs-37994/v1>

License:   This work is licensed under a Creative Commons Attribution 4.0 International License.

[Read Full License](#)

Version of Record: A version of this preprint was published at Journal of the Iranian Chemical Society on March 26th, 2021. See the published version at <https://doi.org/10.1007/s13738-021-02235-7>.

Abstract

Today, finding potential therapeutics for COVID-19 caused by the widespread transmission of *SARS-CoV-2* has become a global challenge. Molecular docking investigation of the therapeutic potential of marketed drugs is a fast and cost effective approach to provide a solution to this problem. In this study, docking simulations performed on the reported structure of the virus main protease, *3CLpro*, to identify potential inhibitors. Accordingly, a database of 50 synthetic compounds including approved drugs and those undergoing clinical trials, and 40 natural compounds particularly those employed in traditional Iranian medicine was constructed. The results indicated that the anti-inflammatory drugs, *Licofelone acyl glucuronide* and *delta-bilirubin*, and natural compounds such as *kappa-carrageenan conformer* and *beta-D-galactopyranosyl* with minimal side-effects, according to *in-vitro* studies, are good candidates to block the enzymatic activity of *SARS-CoV-2 3CLpro*. Moreover, the *compound 1* could be a potential drug candidate for *COVID-19* due to its favorable interactions with the *3CLpro*.

1. Introduction

Coronaviruses are enveloped, positive-sense, single-stranded RNA viruses, which in humans range from the mild respiratory tract infections such as common cold to lethal infections such as *Middle East respiratory syndrome coronavirus (MERS-CoV)*, *severe acute respiratory syndrome coronavirus (SARS-CoV)* and *severe acute respiratory syndrome coronavirus 2 (SARS-CoV-2)*. The first discovery of human coronaviruses back to the late 1960s^[1]. The viral spike peplomers created a crown-like morphology on the surface of the virus, which is the basis for naming the coronaviruses^[2]. Coronaviruses particles have enveloped and pleomorphic structure^[3] with the diameter of around 120 nm^[4] and a distinct pair of electron dense shells formed their envelope^[5]. The coronaviruses are protected outside the host cells by their lipid bilayer envelope and nucleocapsids inside them, as well as membrane proteins^[6]. The coronaviruses subfamily is divided into the four genera called *alpha-*, *beta-*, *gamma-* and *delta-* coronavirus^[7]. The *SARS-CoV-2* belongs to the genus *Beta-coronavirus* from group 2B, which represented close to 79% sequence similarity to the *SARS-CoV* according to the next-generation sequencing technology^[8].

Considering the 96% similarity of the *SARS-CoV-2* to a bat coronavirus, it also appears to have originated from bats^[9].

The rapid spread of the *SARS-CoV-2* has sparked alarm worldwide. The outbreak is believed to have begun in Wuhan, China, in late December 2019^[10], although today, the epicenter of the outbreak is Europe. This pathogen was named as *2019 novel coronavirus (2019-nCoV)* by the World Health Organization (WHO)^[11] and later renamed as *SARS-CoV-2* by the International Committee on Taxonomy of Viruses and the causing disease named as *coronavirus disease 2019 (COVID-19)*^[12]. The virus seems to spread from person-to-person very easily, which makes containment efforts difficult. As of April 6,

2020, a total of more than 1,273,990 people have been infected by the *COVID-19* and the total number of deaths reached 69,444 across the world [13].

So far no antiviral agent has been proven for treat human coronavirus infections and preventive vaccines are still being explored. This is while, the outbreak caused massive disruptions to the nations' health and economy. Therefore, the dire need to find potential therapeutic agents is strongly felt. In this regard, many research teams have focused their researches on finding an effective way for the treatment of *COVID-19* as one of the most critical issues of our time. For the first time, Zhu *et al.* determined whole-genome sequence of *SARS-CoV-2* which can help to quickly detect the virus in patients [14]. Then several laboratories have been submitted this whole-genome sequences to *global initiative on sharing all influenza data* [15]. Four major structural proteins have been encoded in coronaviruses: Spike (S) protein, envelope (E) protein, membrane (M) protein, and nucleocapsid (N) protein [16]. The study of biological structures of these proteins in *SARS-CoV-2* is still at a preliminary stage and heretofore only the crystal structure of *SARS-CoV-2 3CLpro (3-chymotrypsin-like proteinase, 3CLpro)* was solved and released (Protein Data Bank code: 6LU7) [17].

According to the target types, the potential anti-coronavirus therapies is subdivided into human cells- and virus-based therapeutics subdivisions. If the human cells were considered as a target, the anti-coronavirus effect could be induced *via* blocking of the human cells signaling pathways which are essential for virus replication [16]. Moreover, the blocking of the entry receptor proteins on the surface of human cells could prevent from virus attachment to the target cells. As instances, the *angiotensin-converting enzyme 2 (ACE2)* was identified as a *SARS-CoV* receptor [18] and the *dipeptidyl peptidase-4 (DPP4)* was identified as a *MERS-CoV* receptor [19]. If the coronavirus was considered as a target, the anti-virus effect could be induced by blocking the receptor-binding domain of virus, hampering viral self-assembly process, preventing the virus RNA synthesis and inhibiting viral replication. The *3CLpro* has a vital role in coronaviruses replication [20], hence, it could be a promising target to develop *anti-SARS-CoV-2* drugs [21].

The *beta*-coronaviruses are proteolytically cleaved to various proteins employing *papain-like protease (PLpro)* and *3CLpro*. The viral polyprotein is cleaved at eleven distinct sites by *3CLpro* and thereby various non-structural proteins are generated that are important for viral replication [20].

Some potential inhibitors were identified against *SARS-CoV3CLPro* and *MERS-CoV3CLPro* according to the structure-activity analysis [22]. Given the vital role of *3CLpro* in the life cycle of the coronaviruses, studying this protein to find therapeutics against the *SARS-CoV-2* could be very important.

Considering the rapidly spreading *COVID-19* pandemic and the utmost importance of rapid access to the safe and effective medicines, molecular modeling investigation of the therapeutic potential of marketed drugs could be a fast and cost effective way to help solve this problem.

Herein, the molecular docking studies were performed on a broad range of reported synthetic drugs and natural compounds employing AutoDock Vina program [23], with the aim of rapid investigating their inhibition potential against *SARS-CoV-2 3CLpro* and ultimately repurposing them as a possible treatment for *COVID-19*.

In this regard, we used *3CLpro* as a target to screen 90 compounds including synthetic compounds (50 compounds) with various pharmacological usage (such as antiviral, anti-inflammatory, anti-HIV, anti-malarial, antibacterial, anticancer, antioxidant, etc.) and natural compounds particularly those employed in traditional Iranian medicine, with its great history of medicine and pharmacy [24], (40 compounds) by virtual screening protocol. The prediction of the inhibition potential of these compounds against *SARS-CoV-2 3CLpro* could allow researchers to increase the likelihood of success for compounds selected for clinical trials after validating their anti-viral effects *in vitro* and *in vivo*.

2. Computational Analysis

2.1. Structures of inhibitors and targets

The information and SDF files of different synthetic and natural *Covid-19* inhibitors were achieved from PubChem and Zinc15 databases and recorded in Table 1 and 2, respectively. The 2D chemical structure of suggested inhibitors are illustrated in Figure 1 and 2 followed by ChemDraw Professional V15.0 drawing and analysis. The library converted subsequently to PDB files by using Open Babel. The PDB files state the 3D coordination of constituent atoms and chemical bonding. The particular programs within Open Babel enable the software to minimize the input files and select the conformer with lowest energy by systematic determination of conformations and calculation of their *in vacuo* free energy [25]. The structural file of target molecule (*3CLpro*, PDB ID: 6LU7^[17]) was fetched out from RCSB PDB (www.rcsb.org/pdb) with resolution of 2.16Å. It is edited by removing the hetero atoms like water and ligand molecules followed by adding polar hydrogens. From here, Auto-Dock Tools 1.5.6 (ADT) was used to do all the pre-processing steps according to the more reports [26].

Table 1. The physical information and pharmaceutical activities of several drugs and a number of chemical compounds from different resources as *3CLpro* inhibitors

No	Name/ Comound Cod	No. ^a HBD	No. ^b HBA	HAC	Pharmaceuical function ^c
1	Compound1 CID:134816013	4	6	39	-
2	Licofelone acyl glucuronide CID: 71749786	4	8	39	Anti-inflammatory, relevant inhibitor of CYP2C8
3	Ritonavir impurity H [EP] CID: 66832842	1	8	41	-
4	delta-Bilirubin CID:129320333	4	6	43	Antioxidant
5	Raltegravir CID: 54671008	3	9	32	Anti-HIV
6	Nigericin ZINC000085552063	3	11	51	Anti-microbial & anti-bacterial
7	Pradimicin A ZINC000169346835	11	19	60	Anti-HIV & antifungal
8	Rupintrivir ZINC000003919807	3	9	43	Anti-HRV
9	Lopinavir ZINC000003951740	4	5	46	Anti- HIV & AIDS
10	Adenylyl-(3'-5') ribavirin CID: 196553	7	17	39	Anti- influenza A virus
11	Novobiocin ZINC000076945632	5	11	44	Anti-bacterial
12	Megazone CID: 27624	0	7	37	Anti-inflammatory
13	CHEMBL21082 ZINC000028231984	4	9	44	Anti-HRV
14	Simeprevir ZINC000085540268	2	10	52	Anti-HCV

15	CGP 75136 ZINC000004394015	5	10	50	Anti-HIV
16	Amenamevir CID: 11397521	1	7	34	Antiviral
17	Conivaptan CID: 151171	2	3	38	Inhibitor of antidiuretic hormone
18	CHEMBL140521 CID: 6479024	3	8	43	Anti-HRV
19	Indinavir CID: 5362440	4	7	45	Anti- HIV & AIDS
20	Compound 20 CID: 134814833	3	11	48	Anti-HIV & anti- TB activity
21	Oxaprozin CID: 4614	1	4	22	Anti-inflammatory
22	Telmisartan CID: 65999	1	4	39	Anti-hypertensives
23	Boceprevir CID: 10324367	4	5	37	Anti-HCV
24	Elvitegravir CID: 5277135	2	7	31	Anti-HIV
25	Telaprevir CID: 3010818	4	8	49	Anti-HCV
26	Saquinavir ZINC000003914596	5	7	49	Anti- HIV & AIDS
27	Atazanavir ZINC000003941496	5	9	51	Anti-HIV
28	Maraviroc CID: 3002977	1	6	37	Anti- HIV & AIDS
29	Compound 29	1	10	46	Anti-HIV & anti-TB activity

	CID: 134815433				
30	CHEMBL289920 CID: 6477669	3	9	43	Anti-HRV
31	CHEMBL345023 CID: 6478681	3	8	42	Anti-HRV
32	Geneticin CID: 134688573	10	14	34	Anti-bacterial
33	Ritonavir CID: 392622	4	9	50	Anti-HIV
34	Vancomycin Mimic ZINC000150553684	7	11	75	Antimicrobial
35	Ribavirin 5'- Triphosphate CID: 122108	7	16	29	Antiviral
36	Oseltamivir CID: 65028	2	5	22	Anti-influenza viruses
37	Phenylbutazone CID: 4781	0	2	23	Anti-inflammatory, antipyretic, and analgesic
38	Licofelone CID: 133021	1	2	27	Anti-inflammatory, anti-analgesic
39	Parecoxib CID: 119828	1	5	26	Anti-inflammatory, antipyretic activities
40	Sofosbuvir CID: 45375808	3	11	36	Anti-HCV
41	Lopinavir free Amine CID: 17755107	4	4	34	-
42	Isoxicam CID: 54677972	2	7	23	Anti-inflammatory and anti-rheumatic
43	(1R,2R)-2-azido-1,2-dihydro oseltamivir CID: 76968516	2	7	25	-

44	Etoricoxib CID: 123619	0	4	24	NSAID, antipyretic, analgesic
45	Fingolimod CID: 107970	3	3	22	Immunomodulatory drug, used to treat MS
46	Chloroquine CID: 2719	1	3	22	Anti-inflammatory, antimalarial
47	Firocoxib CID: 208910	0	5	23	Anti-inflammatory & antineoplastic
48	Romidepsin CID: 123135747	4	8	36	Antineoplastic activity
49	Mesalazine CID: 4075	3	4	11	Antiinflammatory
50	Favipiravir CID: 492405	2	4	11	Antiviral

^a The number of hydrogen bond donors

^b The number of hydrogen bond acceptors

^c All of the pharmaceutical function information are recorded from PubCheme except the ligands containing references which are mentioned in supplementary information.

Table 2. The physical information and pharmaceutical activities of *SARS-CoV-2* inhibitors from natural sources

No.	Name/ Comound Cod	No. HBD	No. HBA	HAC	Pharmaceutical function ^a	Source ^a
1	kappa-Carrageenan conformer ZINC96061851	10	25	51	Antiviral activity against myxoviridae, and coronaviridae	Red Algae
2	beta-D- Galactopyranosyl CID: 23656242	9	19	50	Anti-inflammatory	Rosa canina
3	Calycosin 7-O- glucoside CID: 5318267	5	10	32	Antiviral	Astragalus
4	Gallic acid 3- cholesteryl ester CID: 101021751	3	5	39	Antimicrobial activity	Ficus carica
5	Spicoside A CID: 44258517	0	7	30	Neuroprotective potency	Cichorium intybus
6	Corilagin CID: 73568	11	18	45	NSAID, antihypertensive agent	Euphorbiaceae
7	Astragalin CID: 5282102	7	11	32	Anti-inflammatory	Rosa canina
8	Podophyllotoxin acetate CID: 164791	0	9	33	Anticancer, antiviral	Euphorbia
9	Rhamnetin 3-O- beta- glucopyranoside CID: 14704554	7	12	34	-	Syzygium aromaticum
10	Astragalus polyphenol CID: 5321884	7	9	29	Anti-inflammatory antioxidant	Astragalus
11	Geraniin ZINC000169289506	14	27	68	antiviral	<i>Nephelium lappaceum</i>
12	Gallic Acid Tribenzyl Ether	1	5	33	Antimicrobial	Ficus carica

	CID: 11133969					
13	Linalool-3-Rutinoside CID: 21630850	6	10	32	Antibacterial, antifungal and antiviral	Myrtus communis
14	Rhamnopyranoside CID: 21606527	9	15	42	Inhibitor of topoisomerase I and II	Cichorium intybus
15	Catechin gallate CID: 5276454	7	10	32	Anti-inflammatory	Rosa canina
16	Chicoric acid CID: 5281764	6	12	34	Anti-HIV	Echinacea
17	Tiliroside CID: 5320686	7	13	43	Anti-inflammatory	Rosa canina
18	Glycyrrhizic acid CID: 14982	8	16	58	Anti-allergic, antiviral and anti-inflammatory	Licorice
19	Hyperin CID: 133568467	8	12	33	Anti-inflammatory	Rosa canina
20	Licorice glycoside E CID: 101938909	7	14	50	-	Licorice
21	Rosmarinic acid CID: 5281792	5	8	26	Anti-inflammatory, antiviral	Peperminte
22	Syringin CID: 5316860	5	9	26	Immunopotentiating, immunostimulatory, radioprotective	Ginseng
23	Carboxymethyl inulin CID: 446984	3	2	32	-	Cichorium intybus
24	Rutin CID: 5280805	10	16	43	Anti-inflammatory	Rosa canina
25	Quercetin CID: 5280343	5	7	22	Anti-inflammatory	Rosa canina
26	Rhamnetin CID: 5281691	4	7	23	Anti-inflammatory, antioxidant	Syzygium aromaticum

27	beta- Sitosterol CID: 222284	1	1	30	Anti-carcinogenic, anti-atherogenic	Cichorium intybus
28	Sageone CID: 6481824	2	3	22	Anti- HIV-1	Sage
29	Apigenin CID: 5280443	3	5	20	Anti-HSV, Anti-ADV, Anti-HBV	Basill
30	Oleanolic acid CID: 10494	2	3	33	Antiviral, Anti-HIV, Anti-influenza	Rosemary
31	Deoxylactucin CID: 442196	1	4	19	Antifungal,	Cichorium intybus
32	Sambucus nigra Degraded cyanogenic glycosides (2'-Epimer) CID: 131751786	2	9	25	Anti-influenza virus, reducer of upper respiratory symptoms	Black elderberry (Sambucus nigra)
33	Luteine (Xanthophyll) CID: 5368396	2	2	42	anti-inflammatory	Rosa canina
34	Shogaol CID: 5281794	1	3	20	anti-inflammatory, antimicrobial	Ginger
35	Theophylline CID: 2153	1	3	13	Bronchodilator & Vasodilator Agents	amellia sinensis & Coffea arabica
36	Carvacrol CID: 10364	1	1	11	Anti-MNV, Anti-RSV Anti-HSV-1,	Oregano
37	Menthol ZINC000001482164	1	1	11	Anti-inflammatory, antiviral	Peperminte
38	Germacrene D CID: 5373727	0	0	15	Antiviral, antifungal, antibacterial,	Myrtus communis

39	trans-Pinocarveol CID 88302	1	1	11	antimicrobial activity	Erodium cicutarium
40	Diallyl trisulfide ZINC000001531082	0	2	8	Anticancer & antiviral	Garlic

^a All of the pharmaceutical function and sources information are recorded from PubCheme except the ligands containing references which are mentioned in supplementary information.

2.2 Preparation of inhibitors and targets

ADT converts PDB files of the ligands and receptors to the AutoDock Vina program [23]. We use Vina in this study, inputs in PDBQT format during the process naming the preparation of inhibitor and targetstructures. In this way, the PDB format extended to PDBQT via addition of partial charge and atom type to ATOM and HETATM records and recording the information of molecule rigid blocks. For the rigid docking running in this study, the rotatable bonds of ligand explicitly changed to non-rotatable bonds.

2.3 Molecular docking study

Molecular docking was performed using Vina program, version 1.1.2 on Windows 8.1 plat form (64-bit) with Asus X450C machine (Intel Pentium ULV 1.8 GHz, 4 GB memory). After preparing the PDBQT files, it is require to adjust the size and center point of a 3D box for ligand docking. In the set of ligands docked to the receptor, the grid center was selected as the middle point between extreme value of x, y, and z coordinates. The grid dimensions were chosen so as to include all atoms of the ligand set, and then augmented by 10 Å in $\pm x$, $\pm y$, and $\pm z$ directions [27]. The Num_modes was 50 for each ligand also. The options employed for other parameters were default. In especial, the grid spacing was 1.0 Å.

2.4 Analysis of docking outcome

Vina results, including multiple modes in PDBQT format, describe the docked ligand position, orientation and conformation. However, many visualization programs are not capable to read these files with nonstandard format, AutoDock Tools, discovery studio and LigPlot are freely available options used to visualize and analyze the Protein–ligand interactions in this project [28].

3. Results And Discussion

Protein-ligand docking is a process in which protein related binding mode and affinity of ligand is predicted. Docking programs, as a key tool in computer-assisted drug design (CADD) and structural molecular biology, generally used for estimating the modeled system free energy and sampling its positional space by using a scoring function and an exploration method, respectively. AutoDock is one of the well established and open source protein-ligand docking softwares available. Moreover, it is an advantaous program in teaching, research anddesigining bioactive compounds. To improve the

performance and accuracy of docking process, Vina is published under a free software license by the same group as AutoDock in 2010 [23] which was used in this project.

3.1 Internal validation of molecular docking

In order to substantiate the validation of docking method, the co-crystal ligand, Figure 3A, extracted from crystal structure of CoV-2019 main protease (6LU7) and re-docked. The binding poses of docked and crystallographic ligands are compared as illustrated in Figure 3B. It can be deduced from the figure 3B that the docking process is valid because the cognate ligand docked in the active site of target like crystallographic ligand with little difference in 3-methyl-2-pyrrolidinone ring benzene motif which is denoted by dash line.

3.2. Molecular docking results

Blocking of the *SARS-CoV-2* main protease, *3CLpro*, to prevent the synthesis of virus RNA and its replication is one of the current suggested therapies for *Covide-19* diseases [29]. Based on the relevant target fetched from PDB, 6LU7, we screened potential bio-active synthetic and natural chemical compounds from PubChem and Zinc database using Vina. The ranking of AutoDock results is based on the lowest binding free energies and RMSD values of determined binding site. On the other hand, in Vina the RMSD value related to the top ranked pose which presents that the highest negative binding energy is 0. Therefore, Vina ranks docking results based on the top ranked binding free energy not the relevant RMSD value [30]. The other binding affinity indicator, ligand efficiency (LE), is the size dependent binding energy and calculated by Eq.(1) [31].

LE = $-\Delta G_b/HAC$ Eq.(1)

Where, ΔG_b stands for calculate binding energy and HAC is heavy atom counts of a ligand, a number of non-hydrogen atoms that expresses ligand size. Based on this parameter, the larger ligand provide more interactions with target and show grater binding energy. However, the ligand efficiency of large ligands are reduced because these compounds interact with other regions beside 'hot spots' and may not necessarily be the most efficient binders [32]. Hence, Vina results to clarify the ligands with highest binding affinity to *3CLpro* are charted for this research based on lowest binding energy not subsequent RMSD values. In the same amount of binding energy, the ligands with higher ligand efficiency are preferred. Results are summarized in Table 3 and Table 4. As shown in Table 3, chemical compound 1, Licofelone acyl glucuronide (antiinflammatory drug), Des(isopropylthiazolyl) hydantoin-oxazolidinone Ritonavir, delta-Bilirubin (antioxidant), Raltegravir (anti-HIV agent), Nigericin (antimicrobial and antibacterial agent) and Pradimicin A (anti-HIV and antifungal agents) had lowest binding energy. A number of other marketed drugs such as Rupintrivir (anti-HRV), Novobiocin (anti-bacterial agents), Megazone (antiinflammatory), Simeprevir (anti-HCV) and Amenamevir (anti- varicella-zoster virus and anti- herpes simplex virus types I & II), showed relatively low binding energy which are worth studying more. However, some others like Sofosbuvir (anti-HCV), Isoxicam (anti-rheumatic), Fingolimod

(immunomodulatory drug used to treat relapsing multiple sclerosis), Romidepsin (antineoplastic activity), and several anti-inflammatory drugs (Etoricoxib, Firocoxib, and Mesalazine) showed highest binding energy. For natural ligands extracted from various sources, Table 4, kappa-Carrageenan conformer, beta-D-galactopyranosyl, Calycosin 7-O-glucoside, Gallic acid 3-cholesteryl ester, Spicoside A, Corilagin, Astragalin, Podophyllotoxin acetate, Rhamnetin and 3-O-beta-glucopyranoside showed lowest binding energy, respectively. Like synthetic ligands, natural ligands with highest estimated ligand efficiency do not have lower binding energy. According to the mentioned results, the small-molecule compounds containing lowest binding energy could probably have the inhibitory potential of *3CLpro* target and used to treat the *SARS-CoV-2*. Based on the different theoretical and clinical studies, several research groups claimed that the Telmisartane ^[29] (anti-hypertensives agent), Conivaptan ^[29] (treatment of hyponatremia), Chloroquine ^[33] (antimalarial), Favipiravir ^[34] (antiviral) and several anti-HIV agents such as Lopinavir ^[35], Indinavir ^[34], Saquinavir ^[36], Ritonavir ^[37] and Atazanavir ^[38] could be the best *3CLpro* inhibitors. Moreover, we docked these marketed drugs to compare them with other research group studies. The data from Table 3 showed that most of these drugs may have relatively acceptable binding affinity to *3CLpro* target, except the Chloroquine and Favipiravir. However, the applied receptor structure and scoring function are the same, the predicted binding constants are non-similar for different research groups. These differences are related to the not only different ligand and receptor preparation parameters but also to the different search procedure. For example, in preparation step, the different assigned charge, relaxation and flexibility of receptor besides the different applied united atoms, added charge type and number of bond torsions for ligand could not provide the same results. In docking step, the exhaustiveness and randomness of the search procedure in addition to the size and centering of the grid box could increase these differences, as well ^[39]. If we want to look on the bright side, the various binding energy estimated by different groups provide valuable information for further computational and experimental studies.

Table 3. The binding energy and ligand efficiency (LE) indices of synthetic ligands docked to *3CLpro* receptor. The binding energy of cognate ligand and ligand efficiency are -13.1Kcal/mol and 0.27, respectively.

No.	ΔG	LE									
1	-10.9	0.23	14	-8.7	0.17	27	-8.3	0.16	40	-7.4	0.20
2	-10.3	0.26	15	-8.7	0.17	28	-8.2	0.22	41	-7.3	0.21
3	-10.0	0.24	16	-8.6	0.25	29	-8.2	0.18	42	-7.3	0.32
4	-9.9	0.23	17	-8.6	0.23	30	-8.2	0.19	43	-7.2	0.29
5	-9.8	0.31	18	-8.5	0.20	31	-8.1	0.19	44	-7.2	0.30
6	-9.8	0.19	19	-8.5	0.19	32	-8.1	0.24	45	-7.1	0.32
7	-9.8	0.16	20	-8.4	0.17	33	-8.0	0.16	46	-6.9	0.31
8	-9.6	0.22	21	-8.4	0.38	34	-7.9	0.10	47	-6.7	0.29
9	-9.5	0.21	22	-8.4	0.21	35	-7.9	0.27	48	-6.7	0.19
10	-9.4	0.21	23	-8.4	0.23	36	-7.7	0.35	49	-5.6	0.51
11	-9.3	0.21	24	-8.3	0.27	37	-7.5	0.33	50	-5.3	0.48
12	-9.0	0.24	25	-8.3	0.17	38	-7.4	0.27			
13	-8.9	0.20	26	-8.3	0.17	39	-7.4	0.28			

Table 4. The binding energy and ligand efficiency (LE) indices of natural ligands docked to *3CLpro* receptor.

No.	ΔG	LE									
1	-11.5	0.23	11	-10.0	0.15	21	-9.3	0.36	31	-7.3	0.38
2	-11.2	0.22	12	-9.7	0.29	22	-8.9	0.34	32	-6.5	0.15
3	-10.5	0.32	13	-9.7	0.30	23	-8.8	0.27	33	-6.5	0.15
4	-10.2	0.26	14	-9.7	0.23	24	-8.8	0.20	34	-6.0	0.30
5	-10.2	0.34	15	-9.7	0.30	25	-8.7	0.39	35	-5.16	0.43
6	-10.2	0.23	16	-9.6	0.28	26	-8.4	0.36	36	-5.2	0.4
7	-10.2	0.34	17	-9.5	0.22	27	-8.4	0.28	37	-5.1	0.4
8	-10.1	0.31	18	-9.4	0.16	28	-8.0	0.36	38	-5.1	0.34
9	-10.1	0.30	19	-9.4	0.28	29	-7.9	0.39	39	-4.6	0.42
10	-10.0	0.34	20	-9.3	0.19	30	-7.9	0.24	40	-3.5	0.44

3.3. Analysis of molecular docking results

The *3CLpro* or *Nsp5*, the *COVID-19* main protease, which has important role in virus RNA synthesis and replication is one of the most important targets for the introduction of efficient small-molecule inhibitors. The target consist of I, II and III domain identified by residues 1–101, residues 102–184 and residues 201–301, respectively. A long loop between domains II and III and the active site between domains I and II are the other characteristics of *3CLpro* target^[40]. The interactions of *3CLpro* target with reference ligand, N3, and suggested bioactive inhibitors are discussed in the coming sections. For comparison, the 2D images of crystallographic and re-docked ligands interaction with active site of receptor are illustrated in (Figure S1). The further hydrogen bond between N₅ of methyl-2-Pyrrolidinone motif in cognate ligand and Glu166 is a cause of distinct difference between crystallographic and cognate one which is identified by dashed red cycle in Figure 3. The other indistinct differences are include hydrophobic interactions between C₈ and C₁₇ with Pro168 and Met165, respectively. This means the physiological conditions especially various solvents may influence on the ligand-protein interactions in crystal structure.

3.3.1 Synthetic compound analysis

The similarity of binding mode for potentially more effective inhibitors containing lower binding energy was further investigated. The chemical compound 1 with lowest binding energy (–10.9 Kcal/mol) showed relatively similar binding mode but Licofelone acyl glucuronide with binding energy of –10.5 Kcal/mol showed less similar binding mode in comparison to reference ligand (Table3, Figure4). The superposition images of [Ritonavir impurity H \[EP\]](#) and delta-Bilirubin illustrated their lower binding similarity modes, as well (Figure S2).

It is surprising that, Raltegravir (anti HIV agent) with highest binding energy (–9.8 Kcal/mol) toward the above mentioned compounds has more binding mode similarity and could be one of the best candidate drugs for *SARS-CoV-2* (Table3, Figure 5A).

In other research studies, the marketed drugs such as Lopinavir, Indinavir, and Ritonavir have been reported as potential inhibitors to block *3CLpro* of *SARS-CoV-2*. The results of this study containing molecular docking and binding mode similarity based on the X-ray crystallographic structure of Mpro, are compatible with the other predictions^[37] (Table 3, Figure S3). However, Ritonavir with an estimated binding energy of –8.0 kcal/mol could be the best candidate drug due to high similarity of binding mode.

The detailed investigation of ligand and receptor interactions uncover the affinity of suggested inhibitors and facilitate the chance of introducing potential drug candidates for Mpro blocking. As shown in Figure 6A and Figure S4A the compound 1 fitness with active pocket of receptor is well. A number of π – π and π –alkyl hydrophobic interactions between ligand and amino acids such as Gln189, Gln166, His41, Cys145, His164, Met165, Met49, Arg188 and Asp167 conform the compound in the pocket of receptor. The predicted hydrogen bonds of Asn142 with oxygen atoms and Thr26 with hydrophilic hydrogen atom of the compound, guarantee the conformer stabilization, also. The presence of 4 hydrogen bond donor

and 6 hydrogen bond acceptor atoms in the ligand structure and hydrophilic amino acids provide these hydrophilic environment (Table1 and Figure7A).

Anti-inflammatory drug Licofelone acyl glucuronide which is the relevant inhibitor of CYP2C8 [41] was predicted to bind to *3CLpro* with low binding energy (Scores = -10.3 Kcal/mol). The generated docking model shows that the drug conjunction with the active site of the enzyme is created by hydrogen bond between hydroxyl group of drug and Glu166 (Figure 6B, and Figure S4B). Moreover, lots of interactions between drug and hydrophobic amino acids, like His41 (π -sigma), Met49 (π -sulfur, and Cys145 and Met165 (Alkyl & π -alkyl) imply that it may be a potent *3CLpro* inhibitor. The Figure 7B shows the 3D image of provided hydrophobic environment.

The other compound, Ritonavir impurity H [EP], with docking scoring of (-10.0 Kcal/mol) was well fitted into the active pocket of *3CLpro*, also. The Hydrogen bonds between Gln189 and Ser46 with the carbonyl group of the compound and the hydrophobic bonds between ligand atoms and Leu141 (Amide- π stacked), Cys145 (π -alkyl) and His164 (Carbon hydrogen bond) stabilize the ligand conformation and introduce it as a good inhibitor for target (Figure 6C and Figure S4C).

Moreover, the results of delta-Bilirubin docking in the active site of *3CLpro* were analyzed and the output was illustrated in Figures 6D and Figure S4D. The images show two hydrogen bond between ligand N-H groups and Gln189 and Leu167, a π -anion bond between 5member ring of ligand and Glu166 and several alkyl and π -alkyl bonds related to for example, Cys145, Met165 and Met49. This hydrophobic environment besides two hydrogen bond could ensure the stability of ligand and receptor complex. Our findings revealed that all of the analyzed compounds possess docking sites that strongly overlap with the protein pockets, and could be potential therapeutic agents.

Moreover, the marketed drugs like Lopinavir and Indinavir provide more hydrophilic and hydrophobic interactions with different aminoacids, there Figures are not shown in this study, and conform their stabilization in the pocket. According to Table1, Ritonavir with 4 hydrogen bond donor and 9 hydrogen bond acceptor atoms, provide no more hydrogen bonds with amino acids and has less hydrophobic interactions and consequently it could not be stabilized in the pocket of target. Because Licofelone acyl glucuronide, delta-Bilirubin, Lopinavir and Indinavir have been used in clinical practices with limited toxicity, we recommend them to treat *COVID-19*.

3.3.2. Analysis of natural ligands

According to the docking results, lots of natural compounds from different sources were predicted to be *3CLpro* inhibitors with high binding affinity (Table4) through virtual ligand screening. The binding similarity mode and docking result analysis of a number of these compounds containing highest negative binding energy were studied in detail.

The antiviral activity of kappa-Carrageenan extracted from *Red Algae* against myxoviridae, paramyxoviridae, adenoviridae and coronaviridae increases the chance of this ligand to inhibit the SARS-

Cov-2 main protease^[42]. One of the conformers of this compound, ZINC96061851, with lowest binding energy (-11.5 Kcal/mol) showed similar binding mode when overlapped with reference ligand (Figure 8A).

For beta-D-galactopyranosyl^[43] (-11.2 Kcal/mol) with anti-inflammatory effect, which is extracted from *Rosa canina L.*, the binding similarity mode is relatively good (Figure S5A). *Rosa canina L.*, which is called *Nasrarane vahshi*, is *Rosaceae* family plant and grows Kordestan Province, Iran^[44].

The extracted compound from the Astragalus plant, Calycosin 7-O-glucoside^[45], which is proved to have antiviral activity might be a candidate for inhibiting target showed relatively similar binding mode, as well (Figure S5B).

Cichorium intybus L. is the scientific name of *Asteraceae* family plant, locally called Sechertghi, and find in the north of Iran, Turkmen Sahra^[44]. Spicoside A^[46], plant extract, which has the Neuroprotective potency docked into the relevant target and gained -10.2 Kcal/mol binding energy. Unfortunately, the similarity of binding mode for this ligand was lower. The superposition figure of binding mode similarity for this ligand is not shown in this study.

Ficus carica L. is another Iranian medicinal plant that grows in Golestan, Fars and Khuzestan Province and locally called *Anjeir*^[44]. The plant extract, Gallic acid 3-cholesteryl ester^[47], which proven antimicrobial activity showed well binding affinity and higher similar binding mode when docked to *3CLpro* receptor (Figure 8B).

The 2D images of docking result analysis for beta-D-galactopyranosyl are illustrated in Figure 9A and Figure S6A. It can be inferred from the images that the hydroxyl and carboxyl groups of ligand provide hydrogen bonds with Ser46, Leu141, Gln189 and Glu166. The presence 9 hydrogen bond donor and 19 hydrogen bond acceptor atoms in the ligand structure conform the existence of more hydrophilic bonds in the pocket. The interactions of carbon atoms on the ligand structure with amino acids such as Thr24, Thr26, Glu166 created carbon hydrogen bonds, also. These interactions and other hydrophobic interactions such as π -alkyl one between 5member ring of ligand and Cys145 cause beta-D-galactopyranosyl to be a good inhibitor for target blocking.

The different type of bonds between ligand and receptor based on the Figure 9B and Figure S6B for Calycosin 7-O-glucoside are include:

- Hydrogen bonds from the interaction of Cys145, Ser144, Gly143 and Gln189 with different hydroxyl groups of ligand.
- Unfavorable donor-donor bond for Ser144 and Gly143 and hydroxyl groups of ligand.
- Amid- π stacked of ligand aromatic ring and Gln189.
- Hydrophobic bonds of ligand atoms with Asn142, Met165, Glu166, Thr190 and Ala191.

The further analysis of docking results for Spicoside A illustrated in Figure 9C and Figure S6C that showed more hydrogen bonds between hydroxyl and oxygen groups of ligand and different amino acids including Ser144, Asn142, Thr26, Gln189, Gly143, Lue141 and Cys145. In addition, hydrophobic interactions with Phe140, Thr26, Thr25, Glu166, Asn142 and Cys145 may further direct the favorite conformation of this inhibitor.

The data from Figure 9D and Figure S6D showed three hydrogen bond for Ser46 and one hydrogen bond for Thr24, Thr25 and Thr45. The alkyl bonds between carbon atoms of ligand and Cys145 and Met165 are the other characteristics of analysis of docking results.

It's worth mentioning that, as shown in Figure 10, Thr24, Glu166 and Asn142 formed five hydrogen bonds with the oxygen, hydroxyl and sulphate groups of the kappa-Carrageenan conformer. The hydrophobic interactions between the compound atoms and Leu167, Met165, Thr190, Pro168, Gln189, Cys145, Met49 and Thr26 may further stabilize its conformation (Figure 9B).

The results of analysis indicated that all of the above mentioned compounds could be connected to the active site of target via desirable and strong hydrophilic and hydrophobic bonds. These strong interactions are related to the affinity of compound atoms to various amino acids presence in the conserved region which are the key factors in enzymatic catalysis. The compounds could be suitable and potent substitutes for synthetic drugs to treat new coronavirus infections due to their natural origin and fewer side effects.

4. Conclusion

The emergence of *COVID-19* as a potential global health threat caused massive disruptions to the nations' health and economy. The employment of effective and time-efficient protein-ligand docking process to discover potent anti-*COVID-19* compounds at the shortest possible time is critical. The aim of this study was the construction of 50 synthetic compounds with various pharmacological usage including approved drugs and those undergoing clinical trials, and 40 natural compounds database, molecular docking of selected compounds, and evaluation of their binding interaction against the *SARS-CoV-2 3CLpro*. Accordingly, the compound 1, licofelone acyl glucuronide (antiinflammatory drug), [Ritonavir impurity H \[EP\]](#), *delta*-Bilirubin (antioxidant), Raltegravir (anti-HIV agent), Nigericin (antimicrobial and antibacterial agent) and Pradimicin A (anti-HIV and antifungal agents) had lowest binding energy. For natural ligands, kappa-Carrageenan conformer, *beta*-D-galactopyranosyl, calycosin 7-O-glucoside, gallic acid 3-cholesteryl ester, Spicoside A, Corilagin, astragalin, podophyllotoxin acetate, Rhamnetin and 3-O-*beta*-glucopyranoside showed the lowest binding energy, respectively. Moreover, the results showed that among investigated marketed drugs, Telmisartane, Conivaptan, Lopinavir, Indinavir, Saquinavir, Ritonavir and Atazanavir may have relatively low binding energy. The similarity of binding mode and ligand-receptor interactions were investigated for potential inhibitors, optionally. Compound 1, Raltegravir, kappa-Carrageenan conformer and Gallic acid 3-cholesteryl ester showed higher similarity binding mode, as well. The analysis of ligand-receptor interactions revealed that most studied compounds have the

ability to bind to the target pocket. Overall, the compound 1, [CID:134816013](#), was identified as the best inhibitor of *3CLpro* due to the lowest binding energy, highest similarity mode and more ligand-receptor interactions and introduced to further in-vitro and in-vivo studies. Moreover, the small-molecules like licofelone acyl glucuronide and *delta*-Bilirubin in addition to some of natural compounds with highest negative binding energy could probably have the inhibitory potential of *3CLpro* target and they have the potential to become an anti-*COVID-19* clinical drug.

Declarations

Conflicts of interest

Authors declare that they have no conflict of interest.

Acknowledgement

This work was supported by the “Iran National Science Foundation: INSF”.

References

- [1] aJ. S. Kahn, K. McIntosh, *Pediatr. Infect. Dis. J.* 2005, 24, S223-S227; bC. Geller, M. Varbanov, R. E. Duval, *Viruses* 2012, 4, 3044–3068.
- [2] aJ. Almeida, D. Berry, C. Cunningham, D. Hamre, M. Hofstad, L. Mallucci, K. McIntosh, D. Tyrrell, *Nature* 1968, 220, 2; bL. S. Sturman, K. V. Holmes, *Adv. Virus Res. (Elsevier)*, vol 28, 1983, pp. 35–112.
- [3] C. S. Goldsmith, K. M. Tatti, T. G. Ksiazek, P. E. Rollin, J. A. Comer, W. W. Lee, P. A. Rota, B. Bankamp, W. J. Bellini, S. R. Zaki, *Emerg. Infect. Dis.* 2004, 10, 320.
- [4] A. R. Fehr, S. Perlman, in *Coronaviruses* (Springer), 2015, pp. 1–23.
- [5] B. W. Neuman, B. D. Adair, C. Yoshioka, J. D. Quispe, G. Orca, P. Kuhn, R. A. Milligan, M. Yeager, M. J. Buchmeier, *J. Virol.* 2006, 80, 7918–7928.
- [6] B. W. Neuman, G. Kiss, A. H. Kunding, D. Bhella, M. F. Baksh, S. Connelly, B. Droese, J. P. Klaus, S. Makino, S. G. Sawicki, *J. Struct. Biol.* 2011, 174, 11–22.
- [7] A. C. Wong, X. Li, S. K. Lau, P. C. Woo, *Viruses* 2019, 11, 174.
- [8] aD. S. Hui, E. E. Azhar, T. A. Madani, F. Ntoumi, R. Kock, O. Dar, G. Ippolito, T. D. Mchugh, Z. A. Memish, C. Drosten, *Int. J. Infect. Dis.* 2020; bR. Lu, X. Zhao, J. Li, P. Niu, B. Yang, H. Wu, W. Wang, H. Song, B. Huang, N. Zhu, *Lancet* 2020, 395, 565–574.
- [9] aJ. Cohen, *Science* 2020, 10; bP. Zhou, X.-L. Yang, X.-G. Wang, B. Hu, L. Zhang, W. Zhang, H.-R. Si, Y. Zhu, B. Li, C.-L. Huang, *Nature* 2020, 1–4.

- [10]aD. S. Hui, E. I Azhar, T. A. Madani, F. Ntoumi, R. Kock, O. Dar, G. Ippolito, T. D. Mchugh, Z. A. Memish, C. Drosten, *Int. J. Infect. Dis.* 2020, 91, 264–266; bW. H. Organization, " WHO Statement Regarding Cluster of Pneumonia Cases in Wuhan, China. Beijing: WHO", can be found under *www.who.int*. 2020.
- [11]W. H. Organization, " Laboratory testing of human suspected cases of novel coronavirus (nCoV) infection: interim guidance" can be found under *www.who.int*, 2020.
- [12]W. Ji, W. Wang, X. Zhao, J. Zai, X. Li, *J. Med. Virol* 2020.
- [13]C. COVID, " Global Cases by Johns Hopkins CSSE. Вилучено з" can be found under <https://gisanddata.maps.arcgis.com/apps/opsdashboard/index.html#/bda7594740fd40299423467b48e9ecf6>.
- [14]N. Zhu, D. Zhang, W. Wang, X. Li, B. Yang, J. Song, X. Zhao, B. Huang, W. Shi, R. Lu, *N Engl. J. Med.* 2020.
- [15]Y. Shu, J. McCauley, *Euro Surveill.* 2017, 22.
- [16]B. J. Bosch, R. van der Zee, C. A. de Haan, P. J. Rottier, *J. Virol.* 2003, 77, 8801–8811.
- [17]X. Liu, B. Zhang, Z. Jin, H. Yang, Z. Rao, " The crystal structure of COVID–19 main protease in complex with an inhibitor N3. RCSB Protein Data Bank" can be found under <https://doi.org/10.2210/PDB6LU7/PDB>, 2020.
- [18]aD. P. Han, A. Penn-Nicholson, M. W. Cho, *Virology* 2006, 350, 15–25; bX.-Y. Ge, J.-L. Li, X.-L. Yang, A. A. Chmura, G. Zhu, J. H. Epstein, J. K. Mazet, B. Hu, W. Zhang, C. Peng, *Nature* 2013, 503, 535–538; cW. Li, M. J. Moore, N. Vasilieva, J. Sui, S. K. Wong, M. A. Berne, M. Somasundaran, J. L. Sullivan, K. Luzuriaga, T. C. Greenough, *Nature* 2003, 426, 450–454.
- [19]aA. S. Agrawal, T. Garron, X. Tao, B.-H. Peng, M. Wakamiya, T.-S. Chan, R. B. Couch, C.-T. K. Tseng, *J. Virol.* 2015, 89, 3659–3670; bJ. Zhao, K. Li, C. Wohlford-Lenane, S. S. Agnihothram, C. Fett, J. Zhao, M. J. Gale, R. S. Baric, L. Enjuanes, T. Gallagher, *Proc. Natl. Acad. Sci.* 2014, 111, 4970–4975.
- [20]K. Anand, J. Ziebuhr, P. Wadhwani, J. R. Mesters, R. Hilgenfeld, *Science* 2003, 300, 1763–1767.
- [21]aI.-L. Lu, N. Mahindroo, P.-H. Liang, Y.-H. Peng, C.-J. Kuo, K.-C. Tsai, H.-P. Hsieh, Y.-S. Chao, S.-Y. Wu, *J. Med. Chem.* 2006, 49, 5154–5161; bB. Xia, X. Kang, *Protein Cell.* 2011, 2, 282–290; cD. Needle, G. T. Lountos, D. S. Waugh, *Acta Crystallogr., Sect. D: Biol. Crystallogr.* 2015, 71, 1102–1111.
- [22]aT. Pillaiyar, M. Manickam, V. Namasivayam, Y. Hayashi, S.-H. Jung, *J. Med. Chem.* 2016, 59, 6595–6628; bA. K. Ghosh, K. Xi, K. Ratia, B. D. Santarsiero, W. Fu, B. H. Harcourt, P. A. Rota, S. C. Baker, M. E. Johnson, A.D. Mesecar, *J. Med. Chem.* 2005, 48, 6767–6771; cV. Kumar, K.-P. Tan, Y.-M. Wang, S.-W. Lin, P.-H. Liang, *Bioorg. Med. Chem. Lett.* 2016, 24, 3035–3042.

- [23]O. Trott, A. J. Olson, *J. Comput. Chem.* 2010, 31, 455–461.
- [24]aR. E. Dizaji, A. Rezaie kehkhaie, M. Taqi khammar, R. shirazinia, *Int J Plant Sci Hor.*, 2019, 1, 56–62; bA. Ameri, G. Heydarirad, J. Mahdavi Jafari, A. Ghobadi, H. Rezaeizadeh, R. Choopani, *Pharm. Biol.* 2015, 53, 615–623; cJ. Patocka, Z. Navratilova, *Pharmacology* 2019, 20; dM. Farahani, Q. Branch, I. Azad, *Zahedan J. Res. Med. Sci.* 2013, 15, 46–48; eM. Abolhassani, *Arch. Med. Sci.: AMS* 2010, 6, 366.
- [25]G. W. Price, P. S. Gould, A. Marsh, *J. Chem. Educ.*, 2014, 91, 4, 602–604.
- [26]G. M. Morris, R. Huey, W. Lindstrom, M. F. Sanner, R. K. Belew, D. S. Goodsell, A. J. Olson, *J. Comput. Chem.* 2009, 30, 2785–2791.
- [27]T. Gaillard, *J. Chem. Inf. Model.* 2018, 58, 1697–1706.
- [28]A. C. Wallace, R. A. Laskowski, J. M. Thornton, *Protein Eng. Des. Sel.* 1995, 8, 127–134.
- [29]C. Wu, Y. Liu, Y. Yang, P. Zhang, W. Zhong, Y. Wang, Q. Wang, Y. Xu, M. Li, X. Li, *Acta Pharm. Sin. B.* 2020.
- [30]A. Ascone, R. Sakidja, *Int. J. Comput Biol. Drug Des.* 2017, 10, 207–224.
- [31]R. Alikhani, N. Razzaghi-Asl, A. Ramazani, Z. Hosseinzadeh, *J. Mol. Struct.* 2018, 1164, 9–22.
- [32]M. Orita, K. Ohno, M. Warizaya, Y. Amano, T. Niimi, in *Methods in enzymology* (Elsevier), Vol. 493, 2011, pp. 383–419.
- [33]J. Gao, Z. Tian, X. Yang, *Biosci. Trends.* 2020.
- [34]Y.-C. Chang, Y.-A. Tung, K.-H. Lee, T.-F. Chen, Y.-C. Hsiao, H.-C. Chang, T.-T. Hsieh, C.-H. Su, S.-S. Wang, J.-Y. Yu, 2020, DOI 10.20944/preprints202002.0242.v1.
- [35]J. Wang, 2020, DOI 10.26434/chemrxiv.11875446.v1.
- [36]T. Sekhar, 2020, DOI 10.20944/preprints202002.0418.v1.
- [37]Z. Wang, X. Chen, Y. Lu, F. Chen, W. Zhang, *Biosci. Trends.* 2020.
- [38]B. R. Beck, B. Shin, Y. Choi, S. Park, K. Kang, 2020, DOI 10.1101/2020.01.31.929547.
- [39]L. Masters, S. Eagon, M. Heying, *J. Mol. Graph. Model.* 2020, 107532.
- [40]H. Yang, M. Yang, Y. Ding, Y. Liu, Z. Lou, Z. Zhou, L. Sun, L. Mo, S. Ye, H. Pang, *Proc. Natl. Acad. Sci.* 2003, 100, 13190–13195.
- [41]Y. Ma, Y. Fu, S. C. Khojasteh, D. Dalvie, D. Zhang, *J. Med. Chem.* 2017, 60, 8691–8705.

[42]A. a. P.-G. Grassauer, Eva, US, 2009.

[43]K. Winther, A. S. V. Hansen, J. Campbell-Tofte, *Botanics* 2016, 6, 11.

[44]M. Asadi-Samani, M.-T. Moradi, M. Bahmani, M. Shahrani, *Int.J. PharmTech Res.* 2016, 9, 427–434.

[45]H. Zhu, Y. Zhang, G. Ye, Z. Li, P. Zhou, C. Huang, *Biol. Pharm. Bull.* 2009, 32, 68–73.

[46]M. Naoi, M. Shamoto-Nagai, W. Maruyama, *Future Neurol.* 2019, 14, FNL9.

[47]S. Choubey, L. R. Varughese, V. Kumar, V. Beniwal, *Pharm. Pat. Anal.* 2015, 4, 305–315.

Figures

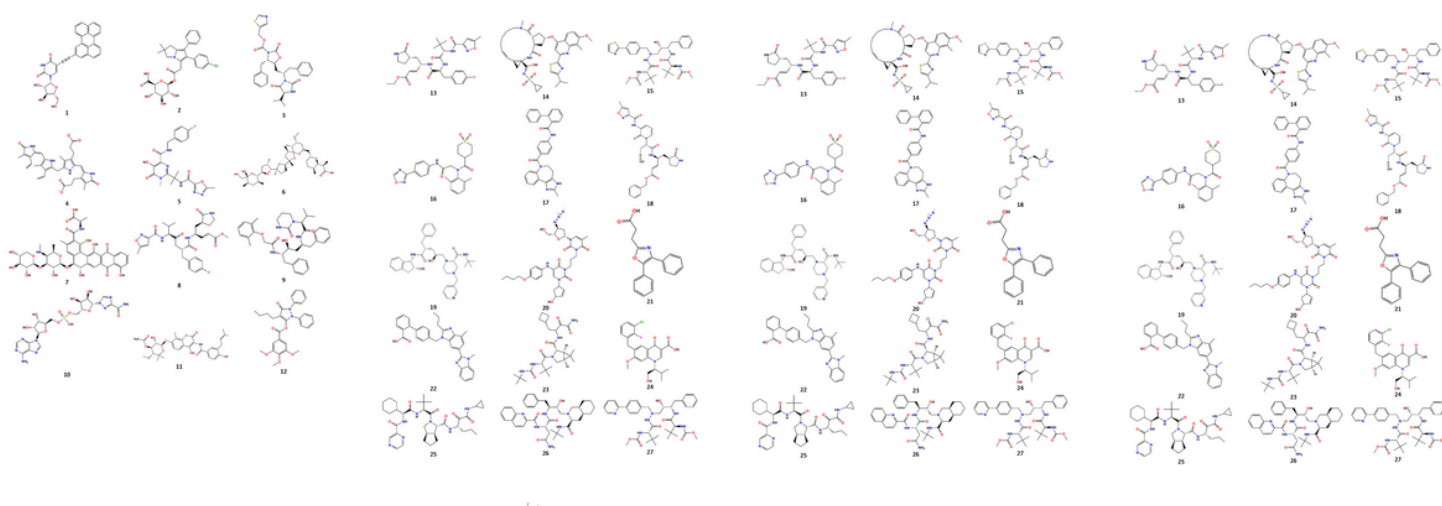
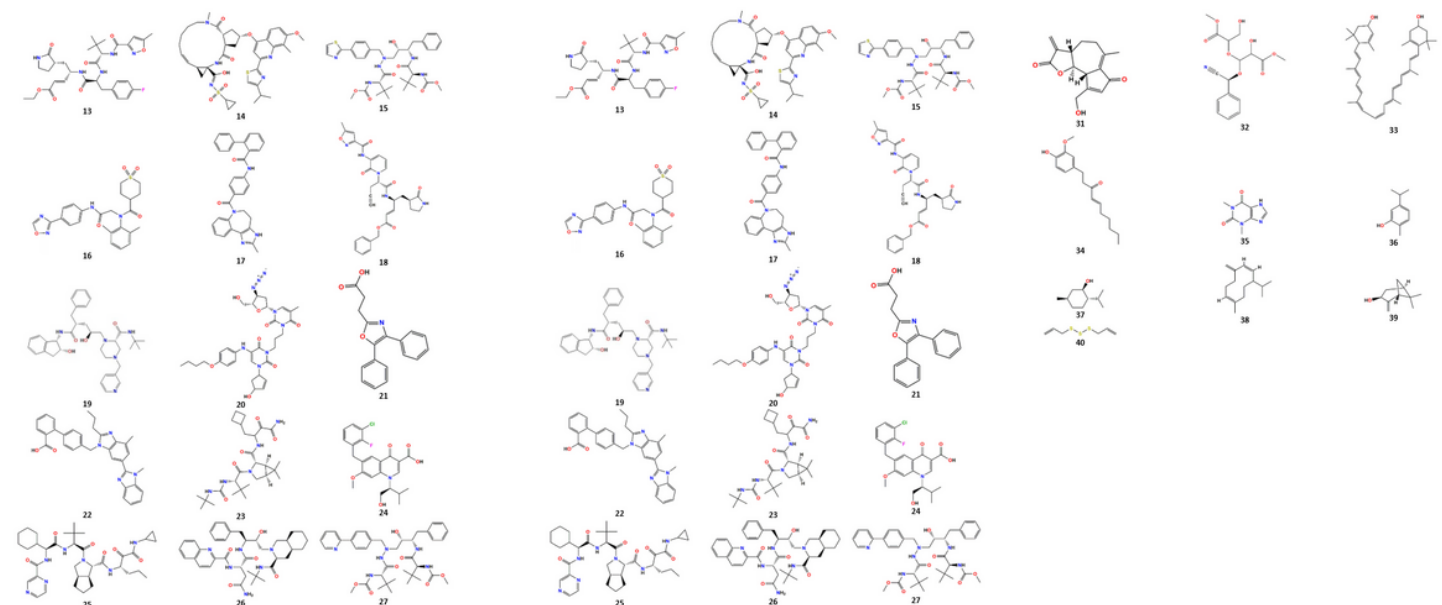


Figure 1

2D structure of synthetic chemical compound as 3CLpro inhibitor candidates



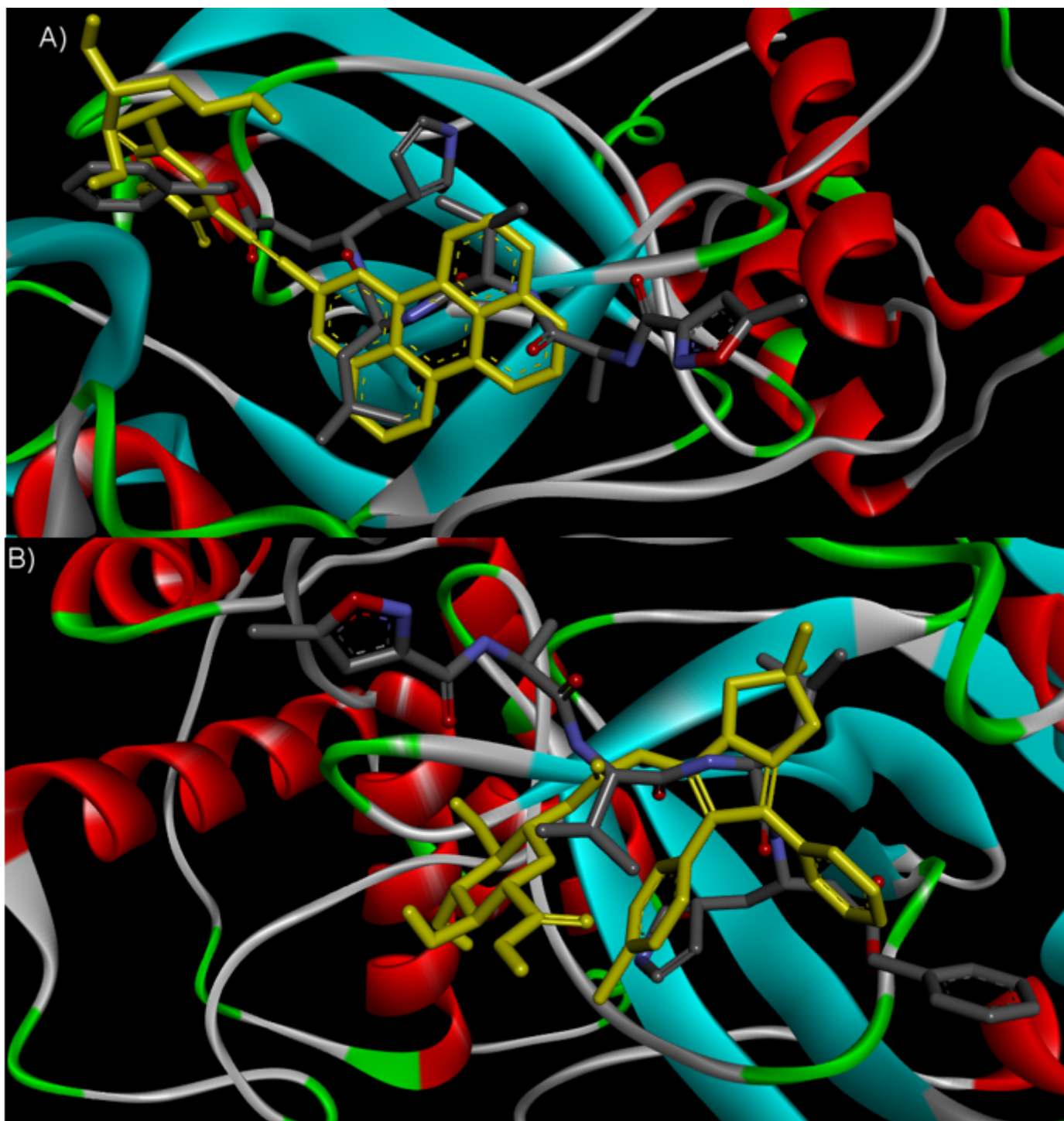


Figure 4

The overlap images of crystallographic binding mode of ligand N3 (●) and predicted binding mode of potential inhibitors (●). A) Compound 1, B) Licofelone acyl glucuronide

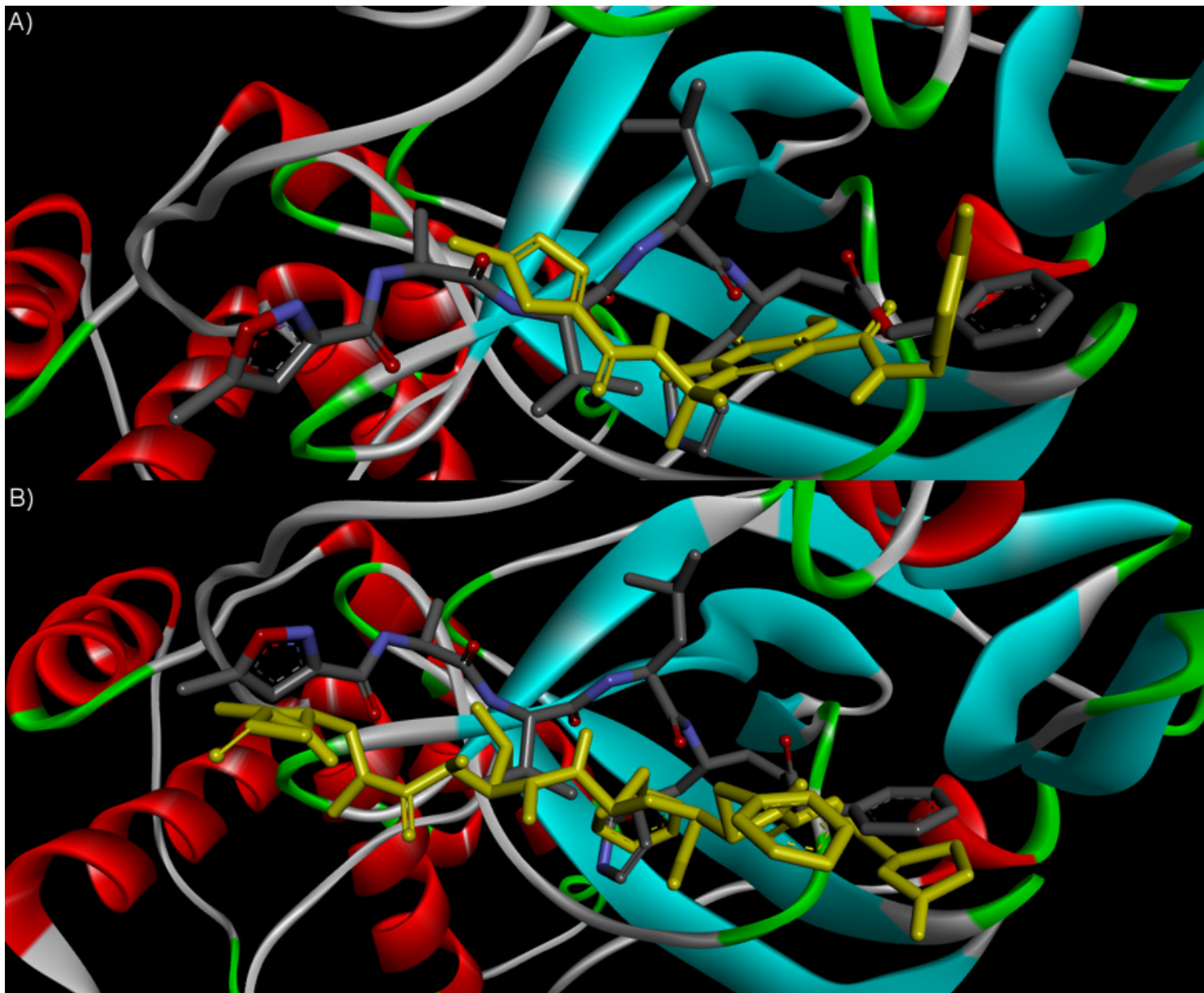


Figure 5

The overlap images of crystallographic binding mode of ligand N3 (●) and predicted binding mode of potential inhibitors (●). A) Raltegravir and B) Ritonavir.

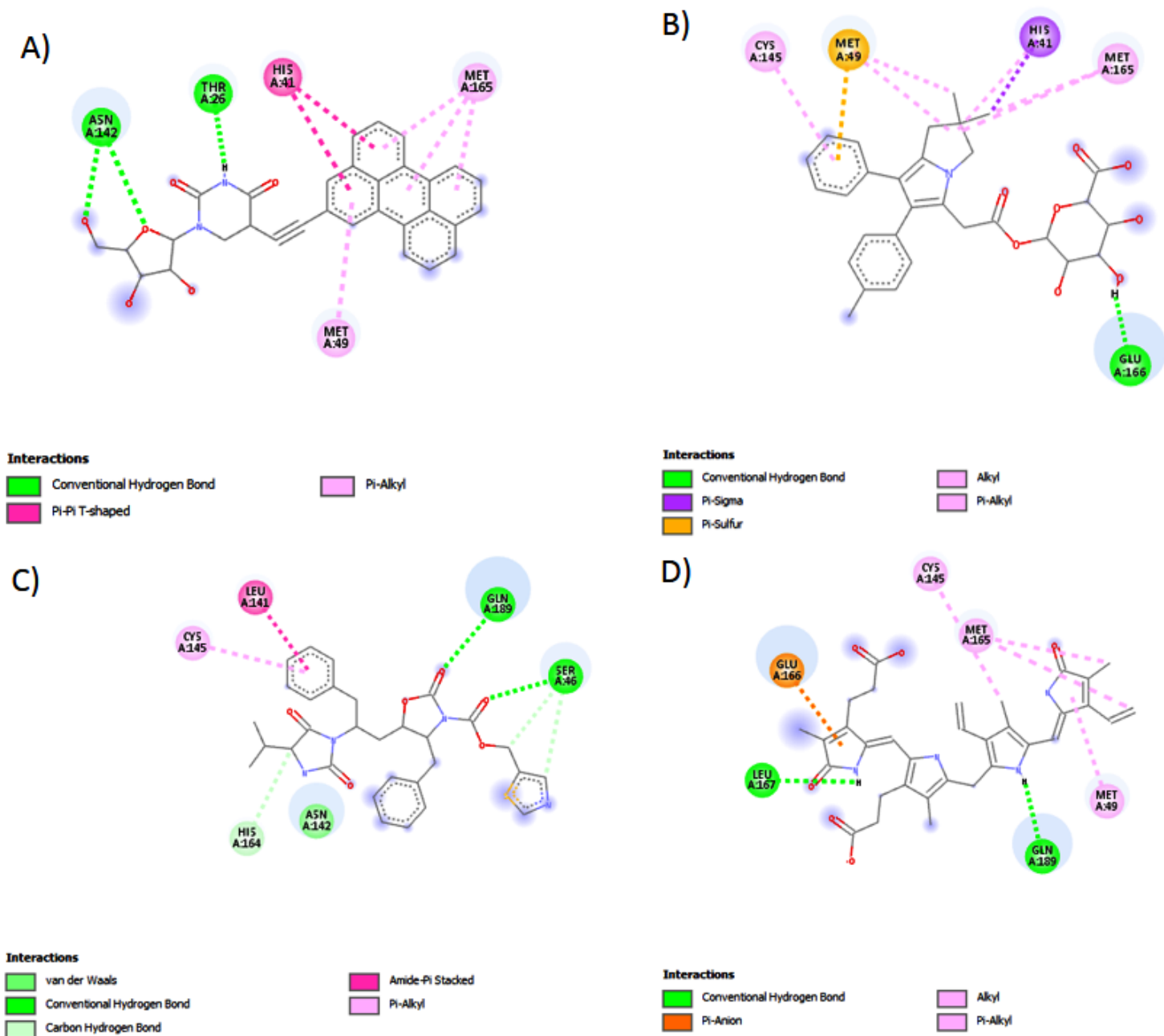


Figure 6

Docking result analysis for synthetic inhibitors: The 2D image of A) Compound 1, (B) Licofelone acyl glucuronide, (C) Ritonavir impurity H [EP] and (D) delta-Bilirubin.

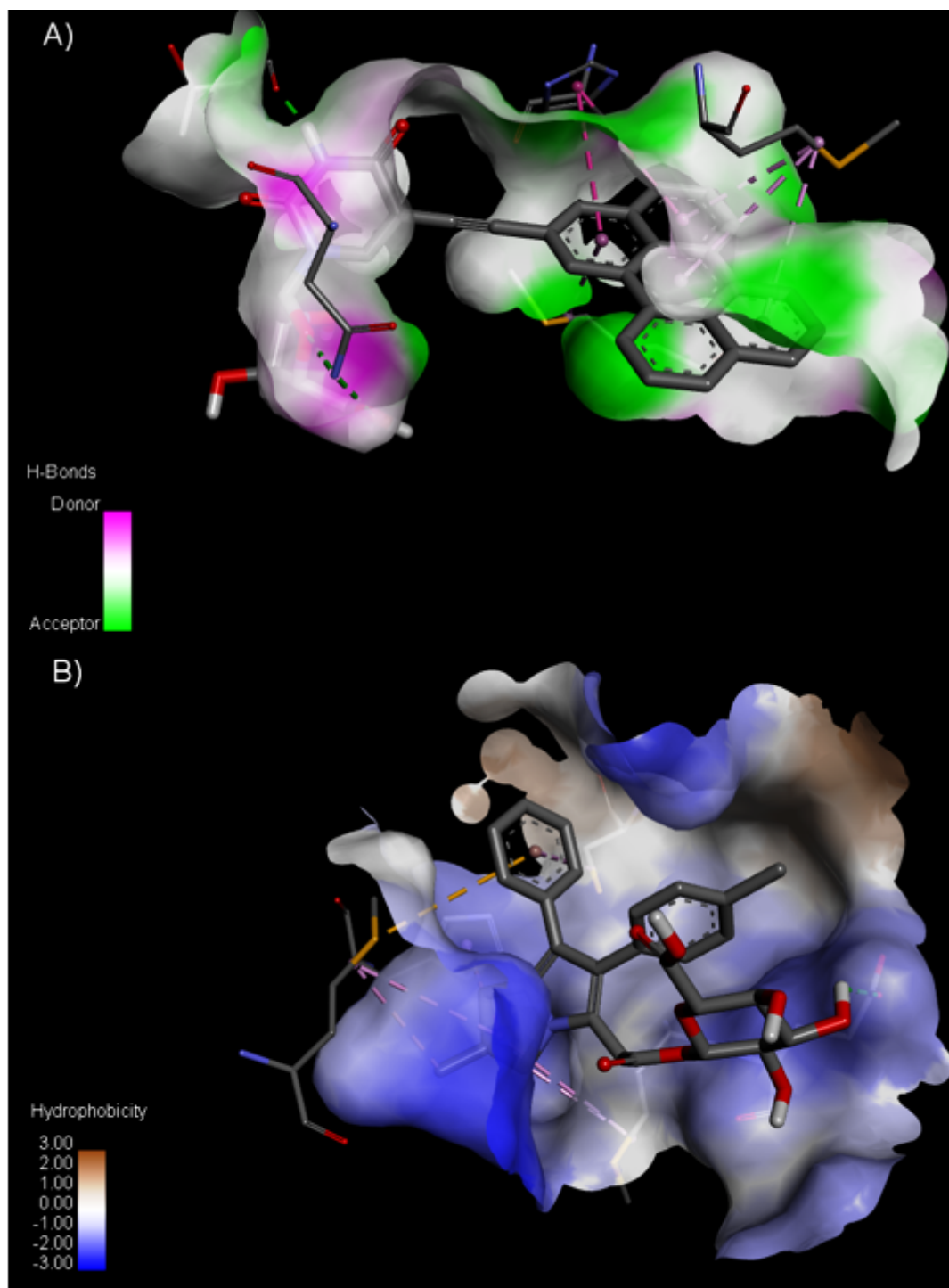


Figure 7

The 3D image of (A) the hydrophilic environment created by Compound1, and (B) the hydrophobic environment created by Licofelone acyl glucuronide.

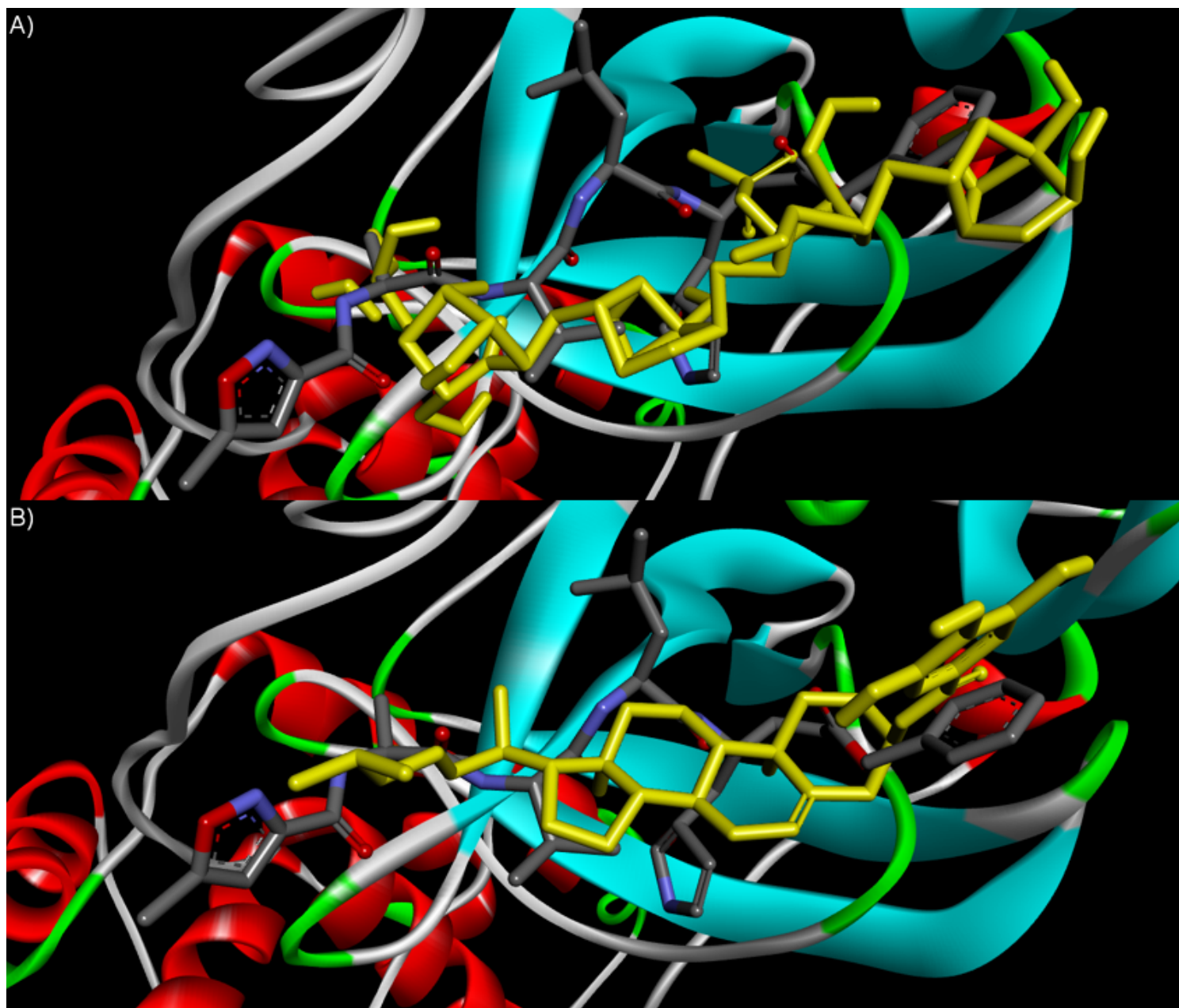


Figure 8

The overlap images of crystallographic binding mode of ligand N3 (●) and predicted binding mode of potential inhibitors (●). A) kappa-Carrageenan and B) Gallic acid 3-cholesteryl ester.

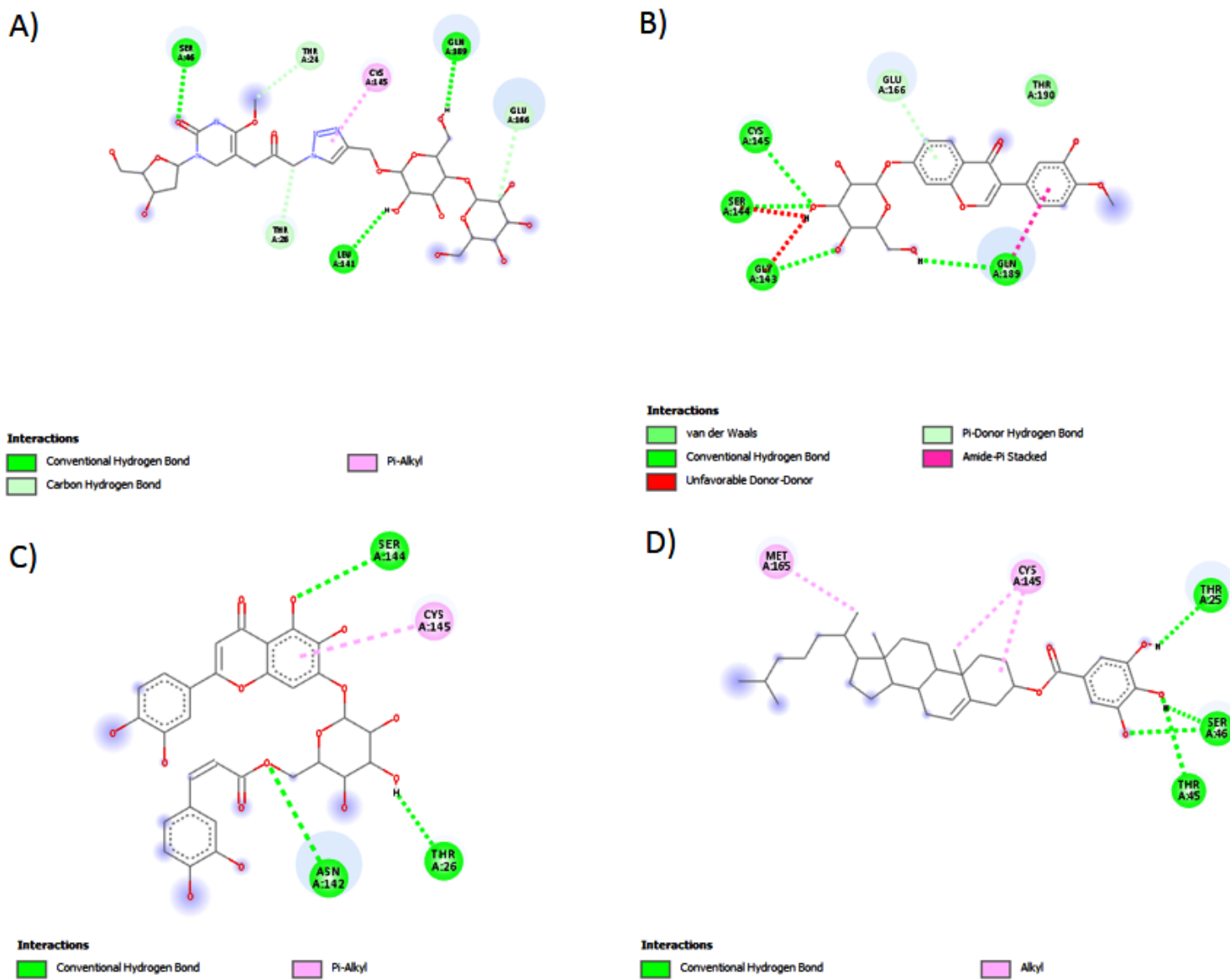


Figure 9

Docking result analysis for natural inhibitors: 2D images of (A) beta-D-galactopyranosyl, (B) Calycosin 7-O-glucoside, (C) Spicoside A, and (D) Gallic acid 3-cholesteryl ester.

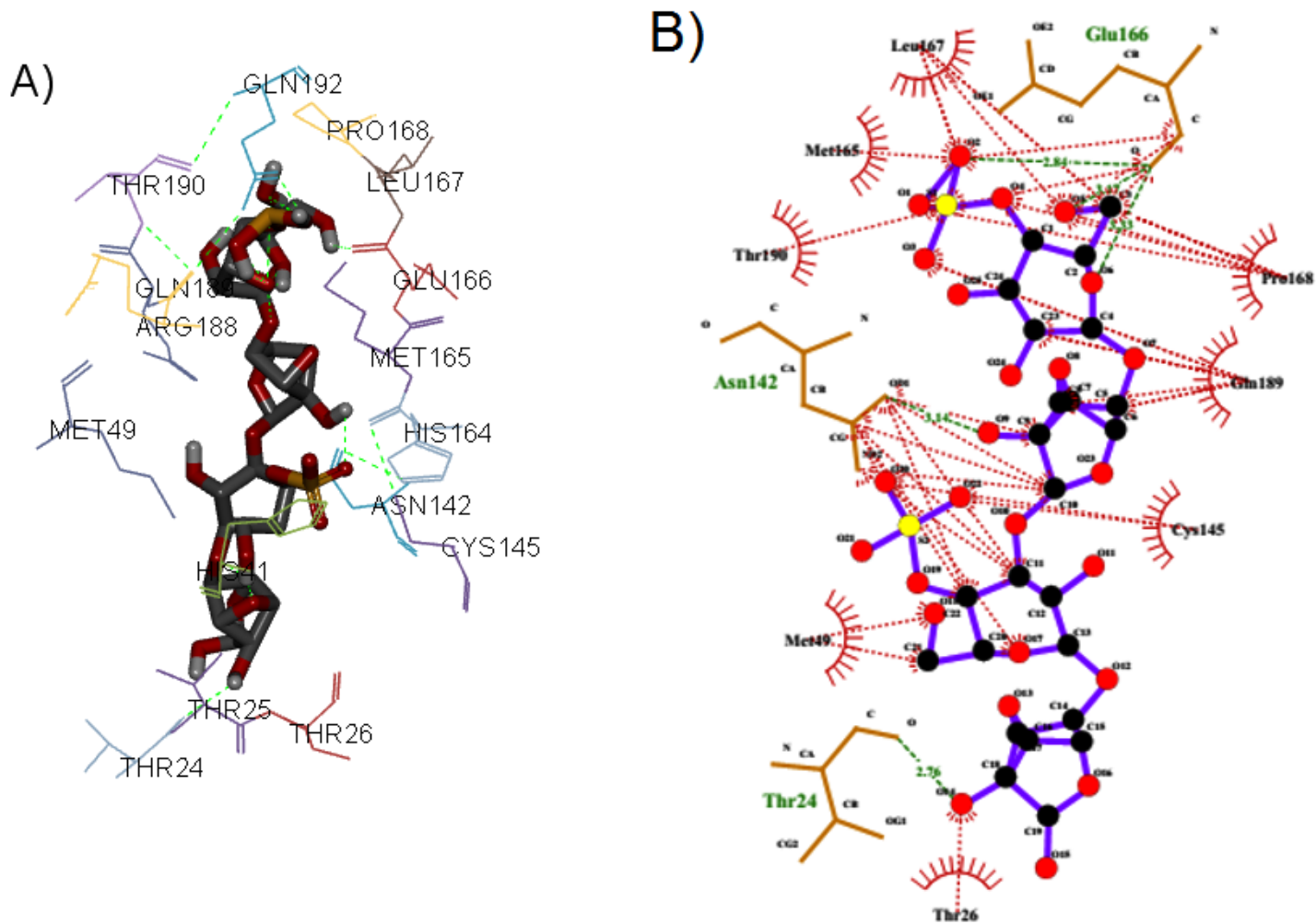


Figure 10

Kappa-Carrageenan conformer-receptor interactions: A) 3D and B) 2D images.

Supplementary Files

This is a list of supplementary files associated with this preprint. Click to download.

- [SupportingInformation.docx](#)
- [GraphicalAbstract.tif](#)